J. COMBIN. MATH. COMBIN. COMPUT. 127a (2025) 5107--5124

Journal of Combinatorial Mathematics
and Combinatorial Computing
www.combinatorialpress.com/jcmcc

Combinatorial Press

Uncertainty modeling and decision optimization of robot vision-guided unloading system based on fuzzy mathematical approach

Fei Yuan[1,✉], Xianzhong Jiang[1], Jingkui Li[1]

[1] *Wuxi Vocational and Technical College of Commerce, Wuxi, Jiangsu, 214153, China*

ABSTRACT

In recent years, it has become the frontier and hotspot of research in the field of intelligent robotics. In this study, a robot vision-guided unloading system is designed, and a robot grasping control method based on fuzzy mathematical method is proposed for the robot unloading problem under the uncertain information environment, and the particle swarm optimized fuzzy PID control algorithm is introduced into the grasping force control field. Comparison experiments of robot joint trajectory tracking, position and control inputs are carried out in the simulation environment, and the method in this paper can realize accurate tracking of motion trajectory and weaken the vibration phenomenon. The robot unloading experiments show that the success rate of single target and multi-target grasping and placing are both above 91% and 85% respectively, which verifies the effectiveness of the particle swarm fuzzy PID control algorithm of this paper in robotic grasping, and it has a certain value of engineering application for robotic unloading control.

Keywords: fuzzy mathematics, particle swarm algorithm, fuzzy PID, visual guidance, robot unloading

1. Introduction

With the improvement of intelligent control technology and mechanical design level, the state constantly encourages the development of intelligent manufacturing, and successively put forward industry 4.0 and "Made in China 2025", to realize the upgrading of manufacturing industry [1-2]. Continuous casting as an advanced casting method in the iron and steel industry production process, the development of its intelligence is also one of the key links in the transformation of the iron and steel industry. In the past, the development of continuous casting process intelligence is limited by the operating environment is high temperature, high dust, high noise, high radiation high-risk areas, industrial robots and machine vision in the iron and steel metallurgy industry development is slow

✉ Corresponding author.
E-mail address: yuanfei@wxic.edu.cn (F. Yuan).

Received 25 February 2024; Revised 10 May 2024; Accepted 15 December 2024; Published Online 15 April 2025.
DOI: 10.61091/jcmcc127a-288

[3-6]. In order to actively respond to the call of national policy and the trend of intelligent development, after continuous improvement and breakthroughs in recent years, artificial intelligence technology has penetrated into the various processes in the steel mill, including temperature measurement and sampling robot running in high temperature and dusty environment, handling and palletizing robots that can adapt to the large weight, high tempo, high frequency, slag replenishment robots can scientifically quantify the demand of the production line, and the stable and fast coating of the Coding robot and so on [7-10].

On the other hand, along with the gradual acceleration of the development process of global economic integration, the rapid rise of the logistics industry. As an important cargo transfer station, the internal logistics operation efficiency and external throughput capacity of regional depots directly affect the level of their own competition and the economic benefits of the entire transportation chain [11-13]. The introduction of a variety of loading and unloading equipment is the most direct and effective way to achieve the above goals, but its price is expensive, unable to meet the needs of large quantities of purchases. In recent years, the labor cost of loading and unloading goods in regional warehouses has been increasing, in addition to the traditional human work is not only inefficient, but also work intensity [14-15]. The robot for the intensity, high repetitive operating environment can show the advantages of inexpensive, reliable, quality and quantity of uninterrupted work, so the combination of cargo handling and robots, the study of unmanned intelligent loading and unloading methods has become a key topic of high concern in the logistics industry [16-17]. Machine vision can replace the human eye for measurement and judgment, and can effectively improve the flexibility and automation of the operation. Convolutional neural network is a multi-layer feed-forward neural network containing convolution operation, which can directly process the input image and retain all the information of the image in a more complete way, and is widely used in the fields of visual tracking, image recognition, etc [18-19].

Literature [20] designed a modular and reconfigurable software framework to assist in solving the automated container loading and unloading problem, which was tested and summarized in real scenarios, and made a positive contribution to the optimization of automated loading and unloading. Literature [21] describes the dangers and inefficiencies of manual loading and unloading of goods, and proposes the use of sensing technology and robotic actuators to realize the automation and intelligent execution of cargo loading and unloading, which improves the efficiency and safety of cargo loading and unloading to a certain extent. Literature [22] conceptualized the basic analytical framework of parallel loading and unloading system, which can obtain the optimal loading and unloading scheme, and then improve the loading and unloading efficiency. Literature [23] designed a material loading and unloading system with the ability to automatically recognize the angle of the common workpiece by combining a camera, a collaborative arm and a plc-controlled conveyor belt, and the feasibility of the system was confirmed in simulation experiments. Literature [24] envisioned a logistics loading and unloading sequence planning method based on the a-star search algorithm to solve the status quo of material loading and unloading clutter, and the proposed strategy was found to be superior to the traditional strategy in practical tests. Literature [25] integrated visual servo technology and heuristic algorithm based generative adversarial network training to develop a strategy for dynamic loading and unloading of materials by robots, and finally introduced an adaptive dual-rate odorless Kalman filter visual tracking algorithm to improve the stability and real-time performance of visual servo system.

This paper designs a robot unloading system based on visual guidance, describes the overall design of the system framework, combines the robot kinematics analysis, and realizes the coordinate conversion between the camera and the robot through hand-eye calibration. Based on the fuzzy mathematical method, the fuzzy PID control robot unloading system is adopted, and the particle swarm algorithm is used to optimize the initial parameters of the decision-making fuzzy PID control, to improve the cumbersome parameter tuning link of purely using PID algorithm, and to construct the particle swarm fuzzy PID control grasping method. The system model and algorithm are combined in Simulink for modeling, and the specific performance of traditional fuzzy PID control method and particle swarm fuzzy PID control of this paper are compared and analyzed from the three dimensions of the joint trajectory tracking, the joint position error and the joint control inputs, to test the optimization effect of the particle swarm algorithm. After that, an experimental platform is built to take the items in the YCB dataset as the operation objects, and carry out single-objective and multi-objective grasping and placing experiments of the model, to explore the control effect of this paper's method on the unloading operation of the robot.

2. Robot vision-guided unloading system

With the rapid development of global industry, the demand for robot intelligence is increasing. The application of robots at this stage is mainly focused on robot grasping work. Applying deep learning to the field of grasping detection, combining target detection and grasping control, realizing rapid identification and accurate grasping of robots, is of great significance for the application of robots in complex scenes such as industrial manufacturing and logistics handling. As a result, this paper designs a robot unloading system based on vision guidance.

2.1. Overall system design

In order to realize the intelligent unloading work of the robot, a robot grasping system composed of two parts, visual guidance and robot grasping, is designed in this section, and the design framework of the robot visual guidance unloading system is shown in Fig. 1. The visual guidance part mainly includes using the visual sensor to collect the picture of the object and perform image preprocessing, and the robot grasping part mainly includes establishing the camera coordinate system and the robot coordinate system, and completing the matrix conversion between the coordinate systems and the system calibration, as well as the unloading control of the robot.

The vision sensor is the basic hardware of the target detection part, which is the "eye" of the robot to realize the grasping task. The application of vision greatly enriches the information that the robot can perceive, which is conducive to the robot's control decisions and the realization of intelligent grasping. The vision sensor converts optical signals into digital images to provide the positional information of the target object for the robot grasping system. The quality of its acquired images directly affects the difficulty of image processing and the prediction results of the target detection algorithm model. The vision sensor chosen in this paper is a high frame rate binocular camera, which can output uncompressed binocular 720P/960P HD images, suitable for high-precision recognition, three-dimensional vision and other research, which is widely used in pattern recognition, target tracking and other fields.

The selection of the robot needs to meet the requirements of the subject experiment on the grasping load, grasping positioning accuracy and activity space. According to the different structure of the robotic arm can be divided into parallel structure robot and series structure robot two types. Among them, parallel robots generally work faster, but the activity space is smaller, and the tandem robot has a high degree of freedom, the robot's activity space is larger, suitable for flexible grasping and sorting scenes. There are different kinds of grasping objects in the grasping experiments of this project, and there may be complex situations such as occlusion between objects, so the tandem structure robot is chosen.

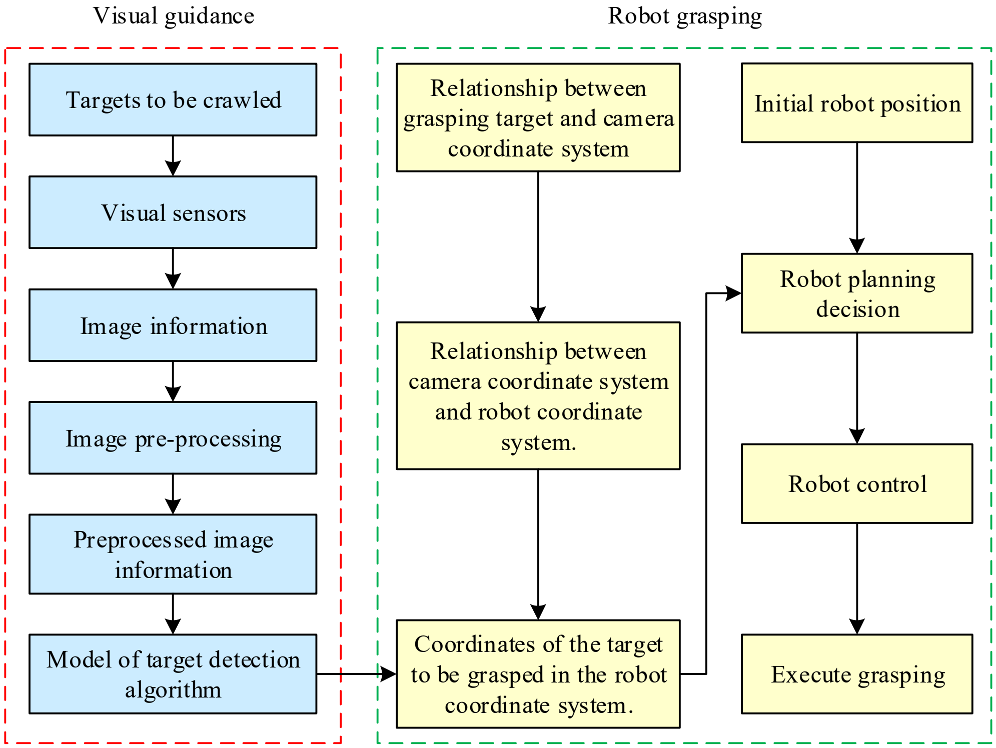

Fig. 1. Design framework of robot visual guidance discharge and loading system

2.2. *Robot vision system calibration*

Robot vision system calibration is one of the key aspects to ensure precise robot motion and control. By analyzing the kinematics of the robot, accurate positioning and control of the target is achieved. Camera calibration is an important step in computer vision and image processing, and calibration removes the aberrations introduced by the camera lens to ensure the accuracy of the image information.

2.2.1. Kinematic modeling. The kinematics of the robot is analyzed using the modified D-H parametric method, where the specific parameters are rod length of a_{i-1}, torsion angle of α_{i-1}, bias of d_i, and turn angle of θ_i.

According to the D-H parametric method the transformation matrix is obtained as:

$$ {}_{i}^{i-1}T = R_{(z_{i-1},\theta_i)} \cdot T_{(z_{i-1},d_i)} \cdot T_{(x_i,\alpha_{i-1})} \cdot R_{(x_i,\alpha_{i-1})} \tag{1} $$

where $R_{(z_{i-1},\theta_i)}$ and $R_{(x_i,\alpha_{i-1})}$ denote rotational transformation matrices and $T_{(z_{i-1},d_i)}$ and $T_{(x_i,\alpha_{i-1})}$ denote translational transformation matrices.

First, its positive kinematic equations are derived. The position of the end-effector of the industrial robot in the global reference system is calculated from the rotation angle of each joint, and the transfer matrix of the end-effector with respect to other coordinate systems ${}_{i}^{i-1}T$ and the transformation matrix between two neighboring joints based on the base coordinate system i are deduced ${}_{i}^{i-1}D$, and finally the position transformation matrix ${}_{i}^{i-1}T$ is obtained.

The corresponding chi-square transformation matrix is derived based on the D-H parameters:

$$D_i = \begin{bmatrix} \cos\theta_i & -\sin\theta_i\cos\alpha_i & \sin\theta_i\sin\alpha_i & \alpha_i\cos\alpha_i \\ \sin\theta_i & \cos\theta_i\cos\alpha_i & -\cos\theta_i\sin\alpha_i & a_i\sin\theta_i \\ 0 & \sin\alpha_i & \cos\alpha_i & d_i \\ 0 & 0 & 0 & 1 \end{bmatrix} \tag{2}$$

From Eq. (1), the coordinate transformation relationship between two consecutive joints can be obtained by substituting the data in the D-H parameter table, and finally the position transformation matrix of the neighboring joints of the robot is obtained ${}^{i-1}_{i}T$:

$${}^{0}_{1}T = \begin{bmatrix} C\theta_1 & -S\theta_1 & 0 & 0 \\ S\theta_1 & C\theta_1 & 0 & 0 \\ 0 & 0 & 1 & 0 \\ 0 & 0 & 0 & 1 \end{bmatrix} \tag{3}$$

$${}^{1}_{2}T = \begin{bmatrix} C\theta_2 & -S\theta_2 & 0 & a_1 \\ 0 & 0 & 0 & d_2 \\ -S\theta_2 & -C\theta_2 & 0 & 0 \\ 0 & 0 & 0 & 1 \end{bmatrix} \tag{4}$$

$${}^{2}_{3}T = \begin{bmatrix} C\theta_3 & -S\theta_3 & 0 & a_2 \\ S\theta_3 & C\theta_3 & 0 & 0 \\ 0 & 0 & 1 & -d_3 \\ 0 & 0 & 0 & 1 \end{bmatrix} \tag{5}$$

$${}^{3}_{4}T = \begin{bmatrix} C\theta_4 & -S\theta_4 & 0 & a_3 \\ 0 & 0 & 1 & d_4 \\ -S\theta_4 & -C\theta_4 & 0 & 0 \\ 0 & 0 & 0 & 1 \end{bmatrix} \tag{6}$$

$${}^{4}_{5}T = \begin{bmatrix} C\theta_5 & -S\theta_5 & 0 & 0 \\ 0 & 0 & -1 & 0 \\ S\theta_5 & C\theta_5 & 0 & 0 \\ 0 & 0 & 0 & 1 \end{bmatrix} \tag{7}$$

$${}^{5}_{6}T = \begin{bmatrix} C\theta_6 & -S\theta_6 & 0 & 0 \\ 0 & 0 & 1 & 0 \\ -S\theta_6 & C\theta_6 & 0 & 0 \\ 0 & 0 & 0 & 1 \end{bmatrix} \tag{8}$$

Eqs. $C\theta_i = \cos\theta_i$, $S\theta_i = \sin\theta_i$.

From Eqs. (3) to (8), the transformation matrix result can be expressed as:

$${}^{0}_{6}T = {}^{0}_{1}T{}^{1}_{2}T{}^{2}_{3}T{}^{3}_{4}T{}^{4}_{5}T{}^{5}_{6}T \tag{9}$$

Secondly, the specific position of the known target point is converted to each joint angle by inverse kinematics equations to accomplish the operations such as wire cutting and wire extraction. The specific positions of the end-effector are p_x, p_y, and p_z, and the postures are r_x, r_y, r_z, m_x, m_y, m_z, a_x, a_y, and a_z. The joint angles are inverted by left-multiplying the inverse matrix of each joint into the position matrix of the industrial robot in a sequential manner.

1) Solving for θ_1. Multiply ${}^0_1T^{-1}$ with ${}^0_6T$ to obtain:

$${}^0_1T^{-1}(\theta_1){}^0_6T = {}^1_2T(\theta_2){}^2_3T(\theta_3){}^3_4T(\theta_4){}^4_5T(\theta_5){}^5_6T(\theta_6) = {}^1_6T \tag{10}$$

The results of θ_1 are as follows:

$$\theta_1 = \arctan\left(p_y / p_x\right) \tag{11}$$

2) Solving for θ_2. After determining the solution for joint angle θ_1, the equation can be obtained by equating the elements $(1,4)$ and $(2,4)$ corresponding to the left and right sides of the matrix of Eq. (9):

$$\begin{aligned} C_1p_x + S_1p_y &= a_3\left(C_2C_3 - S_2S_3\right) - d_4\left(C_2S_3 + S_2C_3\right) + a_2C_2 - p_z \\ &= a_3\left(C_2S_3 + S_2C_3\right) + d_4\left(C_2C_3 - S_2S_3\right) + a_2S_2 \end{aligned} \tag{12}$$

Let $n_1 = C_1p_x + S_1p_y$ be obtained by squaring both sides of Eq. (12) and adding them together:

$$2a_2p_zS_2 - 2a_2n_1C_2 = d_4^2 + a_3^2 - n_1^2 - p_z^2 - a_2^2 \tag{13}$$

Let $2a_2p_z = t_1\cos\varphi$, $2a_2n_1 = t_1\sin\varphi$, then:

$$\begin{cases} \rho = 2a_2\sqrt{p_z^2 + n_1^2} \\ \varphi = \arctan\left(n_1 / p_z\right) \end{cases} \tag{14}$$

Let $n_2 = {d_4}^2 + {a_3}^2 - {n_1}^2 - {p_z}^2 - {a_2}^2$, then the solution of θ_2 is:

$$\theta_2 = \arctan\left(n_2 / p_z\right) - \arctan\left(n_2 / \pm\sqrt{t_1^2 - n_2^2}\right) \tag{15}$$

3) Solving for θ_3. According to the following equation we have:

$${}^0_1T^{-1}(\theta_1){}^1_2T^{-1}(\theta_2){}^2_3T^{-1}(\theta_3){}^0_6T = {}^3_4T(\theta_4){}^4_5T(\theta_5){}^5_6T(\theta_6) = {}^3_6T \tag{16}$$

This leads to θ_3 and t_2:

$$\begin{cases} \theta_3 = \arctan\left(\dfrac{-S\left(C_1p_x + S_1p_y\right) - C_2p_z}{C_2\left(C_1p_x + S_1p_y\right) - S_2p_z + a_2}\right) - \arctan\left(\dfrac{d_4}{\pm\sqrt{t_2^2 + d_4^2}}\right) \\ t_2 = \sqrt{\left(-S\left(C_1p_x + S_1p_y\right) - C_2p_z\right)^2 + \left(C_2\left(C_1p_x + S_1p_y\right) - S_2p_z + a_2\right)^2} \end{cases} \tag{17}$$

Based on the above method, we can find θ_4, θ_5, θ_6. The solutions are as follows:

$$\theta_4 = \arctan\frac{a_x\sin\theta_1 - a_y\cos\theta_1}{\cos\left(\theta_2 + \theta_3\right)\left(a_x\cos\theta_1 + a_y\sin\theta_1\right) + a_z\sin\left(\theta_2 + \theta_3\right)} \tag{18}$$

$$\theta_5 = \arctan\frac{a_x\left(C_1C_4C_{23} + S_1S_4\right) + a_y\left(S_1C_4S_{23} + C_1S_4\right) + a_zC_4S_{23}}{a_xC_1S_{23} + a_yS_1S_{23} - a_zC_{23}} \tag{19}$$

$$\theta_6 = \arctan\frac{-r_x\left(C_1S_4S_{23} + S_1C_4\right) - r_y\left(S_1S_4S_{23} + C_1C_4\right) + r_zS_4S_{23}}{\begin{aligned} &r_z\left(S_5C_{23} + C_4C_5S_2\right) - r_x\left(C_1S_5S_{23} - C_1C_4C_5C_{23} - S_1S_4C_5\right) \\ &-r_y\left(S_1S_5S_{23} - S_1C_4C_5C_{23} + C_1S_4C_5\right) \end{aligned}} \tag{20}$$

where $C_{23} = C_2C_3 - S_2S_3$, $S_{23} = C_2S_3 + S_2C_3$.

2.2.2. Camera calibration. Point P is the specific location of the target in the world coordinate system, and point p is the projection of point P on the image, which corresponds to coordinate (x, y) in the image coordinate system and coordinate (u, v) in the pixel coordinate system.

In imaging, the camera involves four different coordinate systems, the world coordinate system ($O_w - X_w Y_w Z_w$), the camera coordinate system ($O_c - X_c Y_c Z_c$), the image coordinate system ($o - xy$), and the pixel coordinate system ($o_{uv} - uv$).

Transformation from $O_w - X_w Y_w Z_w$ to $O_c - X_c Y_c Z_c$: The world coordinate system P_w (right side) is transformed to the camera coordinate system P_c (left side) by rigid body motion:

$$\begin{bmatrix} X_c \\ Y_c \\ Z_c \end{bmatrix} = R \begin{bmatrix} X_w \\ Y_w \\ Z_w \end{bmatrix} + T \rightarrow \begin{bmatrix} X_c \\ Y_c \\ Z_c \\ 1 \end{bmatrix} = \begin{bmatrix} R & T \\ \vec{0} & 1 \end{bmatrix} \begin{bmatrix} X_w \\ Y_w \\ Z_w \\ 1 \end{bmatrix} = M_1 \begin{bmatrix} X \\ Y \\ Z \\ 1 \end{bmatrix} \tag{21}$$

where R is the third-order rotation matrix, T is the 3D translation vector, and $\vec{0} = (0,0,0)$, M_1 are the simplified fourth-order outer parameter matrices.

Conversion from $O_c - X_c Y_c Z_c$ to $o - xy$: Based on the camera coordinates (X_c, Y_c, Z_c) and the focal length f, the image coordinates can be obtained. The simplification is based on the triangle similarity:

$$\frac{AB}{oC} = \frac{AO_c}{oO_c} = \frac{PB}{pC} = \frac{X_c}{x} = \frac{Y_c}{y} = \frac{Z_c}{z} \rightarrow x = f\frac{X_c}{Z_c}, y = f\frac{Y_c}{Z_c} \tag{22}$$

Convert the above equation to:

$$Z_c \begin{bmatrix} x \\ y \\ 1 \end{bmatrix} = \begin{bmatrix} f & 0 & 0 & 0 \\ 0 & f & 0 & 0 \\ 0 & 0 & 1 & 0 \end{bmatrix} \begin{bmatrix} X_c \\ Y_c \\ Z_c \\ 1 \end{bmatrix} \tag{23}$$

Conversion from $o - xy$ to $o_{uv} - uv$: In the image coordinate system, the x and y axes are parallel to the u and v axes of the pixel coordinate system, respectively. Therefore, these two sets of coordinate systems mainly rely on the translation action to realize the coordinate transformation between each other, the conversion relationship:

$$\begin{cases} u = \dfrac{x}{dx} + u_0 \\ v = \dfrac{y}{dy} + v_0 \end{cases} \tag{24}$$

where dx, dy represent the size of the physical dimensions of each pixel in units of $mm/pixel$, and $\frac{x}{dx}$ and $\frac{y}{dy}$ are calculated in units of pixel.

The coordinates of a point on the image coordinate system are $p(x, y)$ and the image coordinates with respect to its origin (u_0, v_0) are $\left(\frac{x}{dx}, \frac{y}{dy}\right)$. The matrix operator obtained by the transformation solution is:

$$\begin{bmatrix} u \\ v \\ 1 \end{bmatrix} = \begin{bmatrix} \frac{1}{dx} & 0 & u_0 \\ 0 & \frac{1}{dy} & v_0 \\ 0 & 0 & 1 \end{bmatrix} \begin{bmatrix} x \\ y \\ 1 \end{bmatrix} \tag{25}$$

By combining the above equations, the relevant formulae for the interconversion between the world coordinate system and the pixel coordinate system can be deduced as shown below:

$$Z_c \begin{bmatrix} u \\ v \\ 1 \end{bmatrix} = \begin{bmatrix} \frac{1}{dx} & 0 & u_0 \\ 0 & \frac{1}{dy} & v_0 \\ 0 & 0 & 1 \end{bmatrix} \begin{bmatrix} f & 0 & 0 & 0 \\ 0 & f & 0 & 0 \\ 0 & 0 & 1 & 0 \end{bmatrix} \begin{bmatrix} R & T \\ \vec{0} & 1 \end{bmatrix} \begin{bmatrix} X_w \\ Y_w \\ Z_w \\ 1 \end{bmatrix} \tag{26}$$

The simplification yields:

$$Z_c \begin{bmatrix} u \\ v \\ 1 \end{bmatrix} = \begin{bmatrix} f_x & 0 & u_0 & 0 \\ 0 & f_y & v_0 & 0 \\ 0 & 0 & 1 & 0 \end{bmatrix} \begin{bmatrix} R & T \\ \vec{0} & 1 \end{bmatrix} \begin{bmatrix} X_w \\ Y_w \\ Z_w \\ 1 \end{bmatrix} = M_2 M_1 \begin{bmatrix} X_w \\ Y_w \\ Z_w \\ 1 \end{bmatrix} \tag{27}$$

where Z_c is the coordinate of a point in the world coordinate system in the Z -axis direction in the camera coordinate system, and the camera internal reference matrix is M_2, where $f_x = \frac{f}{dx}$, $f_y = \frac{f}{dy}$, and M_1 are the external reference matrices.

Optical aberrations may occur due to the camera lens.

Radial aberrations: At the edges, the camera lens is often unable to avoid significant distortion of the image, which is caused by the “barrel” or “fisheye” effect. It can be expressed by Taylor's formula as follows:

$$\begin{cases} \delta_x(x, y) = x\left(k_1 r^2 + k_2 r^4 + k_3 r^6\right) \\ \delta_y(x, y) = y\left(k_1 r^2 + k_2 r^4 + k_3 r^6\right) \end{cases} \tag{28}$$

Where (x, y) is the original coordinate of the radial undistorted place, $\delta_x(x, y)$ and $\delta_y(x, y)$ are the position after radial distortion correction. k_1, k_2, k_3 indicate the radial distortion coefficient.

Tangential aberration: This is formed when the lens is not strictly parallel to the imaging plane due to defects in the lens manufacturing process. The tangential aberration can be expressed by Taylor's formula with two additional parameters p_1 and p_2 as follows:

$$\begin{cases} \delta_x(x, y) = 2p_1 xy + p_2\left(r^2 + 2x^2\right) + x \\ \delta_y(x, y) = 2p_1\left(r^2 + 2y^2\right) + 2p_2 xy + y \end{cases} \tag{29}$$

Where (x,y) is the original coordinates of the tangential undistorted place, $\delta_x(x,y)$ and $\delta_y(x,y)$ are the positions after correction for tangential distortion. $r^2 = x^2 + y^2$. The equation for the corrected coordinates is shown below:

$$\begin{bmatrix} x' \\ y' \end{bmatrix} = \left(1 + k_1 r^2 + k_2 r^4 + k_3 r^6\right) \begin{bmatrix} x \\ y \end{bmatrix} + \begin{bmatrix} 2p_1 xy + p_2\left(r^2 + 2x^2\right) \\ 2p_1\left(r^2 + 2y^2\right) + 2p_2 xy \end{bmatrix} \tag{30}$$

By calibrating the five parameters k_1, k_2, k_3, p_1, p_2, the lens aberration correction of the camera can be completed, and then the new coordinates of the corrected camera can be obtained x', y'.

2.2.3. Hand-eye calibration. In a real manipulation scenario, once the camera successfully captures the pixel position of the target in the image, a predefined coordinate transformation matrix is applied to accurately convert this position information from the pixel coordinate system of the camera to the spatial coordinate system of the robot end-effector.

The base coordinate system of the robot arm is base, the coordinate system of the robot end-effector is tool, the coordinate system of the camera is camera, and the coordinate system of the calibration board is board, and the transformation relationship between the coordinate systems can be expressed as follows:

$${}_2M_{board}^{cam} * {}_1M_{board}^{cam-1} * M_{tool}^{cam} = M_{tool}^{cam} * {}_2M_{toot}^{base-1} * {}_1M_{tool}^{base} \tag{31}$$

$$\begin{aligned} {}_2M_{board}^{cam} * {}_1M_{board}^{cam\ -1} &= A \\ {}_2M_{tool}^{base-1} * {}_1M_{tool}^{base} &= B \\ M_{tool}^{cam} &= X \end{aligned} \tag{32}$$

$$AX = XB \tag{33}$$

The transformation relationship between the end of the robot arm and its base coordinate system is M_{tool}^{base}, the transformation relationship between the coordinate system of the actuator at the end of the robot arm and the spatial position determined by the camera is M_{tool}^{cam}, the mapping relationship between the spatial position where the calibration plate is located to the camera's coordinate system is M_{board}^{cam}, and the coordinate transformation relationship between the base coordinate system of the robot arm and the calibration plate is M_{base}^{board}. Relying on the internal and external camera parameters derived from the camera calibration to derive X, the coordinate transformation matrix between the end of the robotic arm and the camera.

The pixel coordinate system is transformed to the world coordinate system:

$$\begin{bmatrix} X_w \\ Y_w \\ Z_w \end{bmatrix} = R^{-1}\left(Z_c M_2^{-1} \begin{bmatrix} u \\ v \\ 1 \end{bmatrix} - T \right) \tag{34}$$

$X_w Y_w Z_w$ is the world coordinate system coordinates, R is the external parameter rotation matrix, Z_c is the depth value in the camera coordinate system, M_2 is the internal parameter matrix, u and v are the pixel coordinate system coordinates.

3. Fuzzy math-based robot unloading control

PID control algorithm in the use of the process requires a cumbersome parameter adjustment link, so the fuzzy PID control algorithm is used to control the unloading operation of the robot, on the basis of which the control decision-making optimization is carried out, and the particle swarm algorithm is used to optimize the initial parameters of the fuzzy PID control algorithm offline, and then add them to the fuzzy PID controller, to avoid the disadvantages of setting the initial parameters of the fuzzy PID control algorithm according to experience, and to be able to effectively reduce the overshoot of the control system and reduce the steady-state response time. The following is the gripping control and optimization method of the robot unloading system.

3.1. Fuzzy control

Fuzzy control is a nonlinear control method based on the theory of fuzzy mathematics and fuzzy logic, which has the advantages of no mathematical model and strong robustness compared with traditional control methods. Compared with the traditional exact mathematical model, fuzzy control stands out in its adaptability and fault tolerance to nonlinear and fuzzy systems, and becomes an effective tool for solving complex dynamic systems in real problems.

A fuzzy control system usually consists of three main components: fuzzification, fuzzy inference and defuzzification. In the fuzzification stage, the raw input signals are converted into fuzzy sets to accommodate fuzzy logic processing. This is to deal with the ambiguity and uncertainty in the system inputs. Fuzzy inference is the core part of a fuzzy control system. It uses a set of fuzzy rules, which are based on known experience and knowledge, to generate fuzzy outputs by reasoning through fuzzy logic. After obtaining the fuzzy output, it needs to be mapped back to the actual output, a process called defuzzification. The core idea of fuzzy control is to convert exact control signals and measurements into a fuzzy set of affiliation functions and then apply fuzzy inference rules to generate a fuzzy control output. This output is subsequently defuzzified (i.e., converted to an exact control signal) to drive the controlled system.

The performance and accuracy of a fuzzy logic system can be greatly improved by the correct selection and application of the affiliation function. In practice, determining the affiliation function for the fuzzy characteristics of a research object is a complex and critical process. Choosing the appropriate type of affiliation function is crucial for accurately describing the fuzzy characteristics of the research object. In this section, the algorithm selects the trigonometric function as the affiliation function, which is simpler and more intuitive than other functions, and has a high degree of flexibility that can be adjusted and adapted to the needs. By adjusting the parameters of the trigonometric function, different shapes and widths of the affiliation function can be obtained, so as to better match the data distribution in practical applications.

Trigonometric affiliation function:

$$f(x,a,b,c)=\begin{cases} 0 & x\le a \\ \dfrac{x-a}{b-a} & a\le x\le b \\ \dfrac{c-x}{c-b} & b\le x\le c \\ 0 & x\ge c \end{cases} \tag{35}$$

3.2. Particle Swarm Fuzzy PID Control Algorithm

3.2.1. Transfer function identification. To realize the control of the system, the first need to obtain the system model, the transfer function is a common system representation, because the system in this paper belongs to the black box state, so need to use the transfer function to describe the system. The object grasping process is analyzed, the object should be kept stable in the grasping process, that is, the gravity is balanced with the friction force of the manipulator on the target object.

The force state of the target object during the grasping process is shown in Equation (36):

$$Mg = f_1 + f_2 \tag{36}$$

In the above equation, M is the mass of the object, g is the acceleration of gravity, f_1 and f_2 are the friction forces on both sides of the manipulator, which can be obtained according to the friction force formula (37):

$$f_1 = f_2 = f, f = uF_0 \tag{37}$$

Where, F_0 set the desired gripping force, u for the friction coefficient between the manipulator and the object, determined by the manipulator and the object contact surface material, to prevent the object from slipping calculated to take the friction coefficient of 0.20, will be formula (37) into the formula (36) to obtain the object's force is:

$$Mg = 2uF_0 \tag{38}$$

Finding the grip F_0 for:

$$F_0 = \frac{Mg}{2u} \tag{39}$$

3.2.2. Fuzzy PID control. Using the fuzzy control technique, it is possible to transform the inputs received by the controller into reasonable fuzzy quantities and obtain predictable fuzzy control quantities through reasoning. In addition, through inverse fuzzy control, the parameters of the PID controller can be obtained and can be adjusted in real time as needed, thereby improving the static and dynamic performance of the control system.

r is the given signal of the system input, y is substituted for the system output, e is the error between the system output and the input, ec is the rate of change of the error, K_e and K_{ec} represent the error gain and the rate of change of the error gain, respectively, while the output of the fuzzy control is the amount of change of the fuzzy control parameters. The fuzzy controller can calculate the increment of the next adjustment according to the result of each adjustment and add it with the result of this adjustment as a way to quickly adjust the PID parameters, and its adjustment principle is shown in Equation (40):

$$K_P = K_P' + \Delta K_P, K_I = K_I' + \Delta K_I, K_D = K_D' + \Delta K_D \tag{40}$$

For the realization of fuzzy PID controller, it is mainly to realize the fuzzy controller, and the steps of fuzzy controller realization are as follows:

1) Determine the input and output variables and the domain: firstly, determine the input and output variables of the system, which can be the actual physical quantities or the state variables of the system. In this paper, the inputs of the system are system error e and system error rate of change ec, and after several simulation experiments, we set the system error and error rate of change quantization thesis as $\left[-1,1\right]$, and the output variables as ΔK_P, ΔK_I, ΔK_D represent the increment of the PID controller parameters, respectively, and the quantization thesis is [-3, -3], [-90, -90], [-3, -3].

2) Design of fuzzy process: the input variables are fuzzified into fuzzy sets, and the purpose of fuzzification is to transform the actual variables into fuzzy variables to make them easier to handle. The fuzzification process is usually expressed in the form of fuzzy sets, which is usually accomplished by means of the affiliation function, and common affiliation functions include the triangular affiliation function, the trapezoidal affiliation function and the Gaussian function. In this paper, the more sensitive triangular affiliation function is used.

3) Design fuzzy rule base: general rule base consists of several fuzzy rules within, it is a collection of relationships between input variables and output variables, the establishment of the rule base requires expert knowledge or empirical data, in this paper, a fuzzy rule base is constructed with

reference to a number of literatures. It contains 7 fuzzy subsets, i.e., negative large (PB), negative medium (PM), negative small (PS), zero (ZO), positive small (NS), positive medium (NM), positive large (NB).

4) Perform fuzzy inference operation: fuzzy inference operation is based on matching the input variables with the rule base to derive the output variables of the system. In this paper, fuzzy inference is performed using Mamdan method.

5) Designing the defuzzification process: defuzzification is the process of transforming the defuzzified output into the actual output, and the commonly used methods are the maximum affiliation method, the center of gravity method, and the set average method, this paper uses the center of gravity method to carry out defuzzification, which can effectively avoid the controller jumping phenomenon generated in the defuzzification process, and enhance the control performance of the system, and its basic principle is shown in Eq. (41):

$$v_0 = \frac{\int_V v\mu_v(v)dv}{\int_V \mu_v(v)dv}, V = [-n, n] \tag{41}$$

where v_0 is the center of the region covered by the fuzzy affiliation function $\mu_v(v)$.

6) By combining the above steps together, a complete fuzzy controller is obtained.

3.2.3. Particle Swarm Optimization Decision Making. The input parameters of the fuzzy PID controller can be effectively improved by the particle swarm algorithm, in which the core principles of the particle swarm algorithm include: the size of the particle swarm, the learning factor, the dimensionality, the number of iterations, the inertia weights, and the objective function, which can be effectively adjusted according to different environments, so as to achieve the best control effect. According to the characteristics of the particle swarm algorithm, effective search information can be obtained from the current problem as the beginning of the next round of search, and the selection of the objective function can be made according to the adaptability of the individual in order to achieve the best search effect. Commonly used objective functions include ISE and ISTSE, which are important tools for evaluating whether the objective is optimal or not. Different objective functions have different characteristics, among which ITAE has the optimal response speed in the control system and is suitable for the analysis in the simulation environment, so it is used as the objective function evaluation criterion in this paper, and the ITAE criterion is shown in Equation (42):

$$J = \int_0^\infty t \cdot |e(t)| dt \tag{42}$$

In the process of unloading the object of the robot, the particle swarm algorithm will optimize the initial parameters of the fuzzy controller, so that the fuzzy controller is more in line with the current system, the fuzzy controller at the same time for the dynamic adjustment of the parameters of the PID controller, to obtain superior dynamic performance.

3.3. Simulation Analysis

In order to verify the control performance of the proposed particle swarm fuzzy PID control algorithm, the particle swarm fuzzy PID control robot unloading process is modeled in Simulink, and the traditional fuzzy PID control method is applied to the double-jointed robotic arm on the platform for simulation and comparison observation respectively with this method.

3.3.1. Joint trajectory tracking. Fig. 2 shows the comparison of trajectory tracking curves between traditional fuzzy PID control and particle swarm fuzzy PID control methods, Fig. (a) and (b) show the two-joint trajectory tracking curves under the traditional fuzzy PID control method, and Fig. (c) and (d) show the two-joint trajectory tracking under the particle swarm fuzzy PID control method. The yellow line indicates the desired trajectory, and the blue line indicates the actual trajectory, which shows that both methods can accurately track the desired trajectory after a period of time in the presence of perturbation. The particle swarm fuzzy PID control method in this paper can accurately track the robot joint trajectory in less than 0.5s, while the traditional fuzzy PID control method needs more than 0.5s, and the motion trajectory tracking control effect of this paper's method is more efficient.

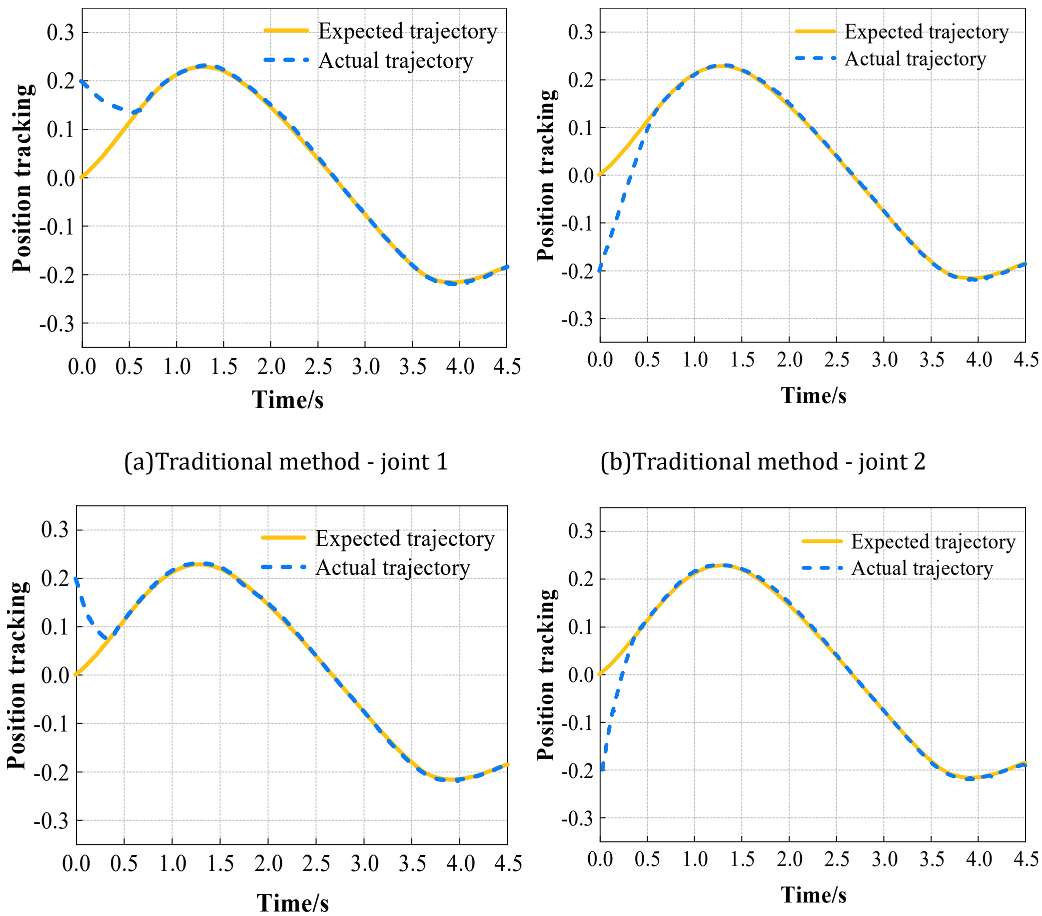

(a)Traditional method - joint 1 (b)Traditional method - joint 2

(c)Our method - joint 1 (d)Our method - joint 2

Fig. 2. Joint trajectory tracking

3.3.2. Joint position error. Fig. 3 shows the comparison of the joint position errors between the traditional fuzzy PID control and the proposed method, Fig. (a) shows the two joint position errors under the traditional fuzzy PID control method and Fig. (b) shows the two joint position errors under the proposed method. The offline calculation of the fuzzy system parameters makes the online calculation of the system reduced, so it can be seen from the comparison in the figure that the proposed method has a faster convergence time compared with the traditional fuzzy PID control, which completes the convergence in 0.5s, and the error range is not much different, and the fluctuation of the error is small, which is within the acceptance range.

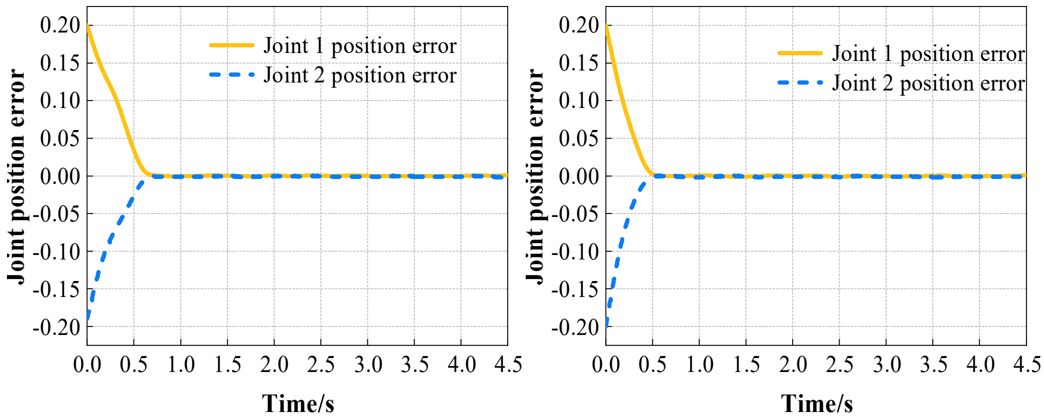

(a)Traditional method (b)Our method

Fig. 3. Joint position error

3.3.3. Joint control inputs. Fig. 4 shows the comparison of the control input curves between the traditional fuzzy PID control and the proposed method, Fig. (a) shows the two-joint control input under the traditional fuzzy PID control method, and Fig. (b) shows the two-joint control input under the proposed method. It can be seen that the traditional fuzzy PID control method has a strong jitter phenomenon and the control input is unstable, while the proposed method optimizes the fuzzy PID controller through the particle swarm algorithm, which greatly reduces the control input jitter and achieves the design goal.

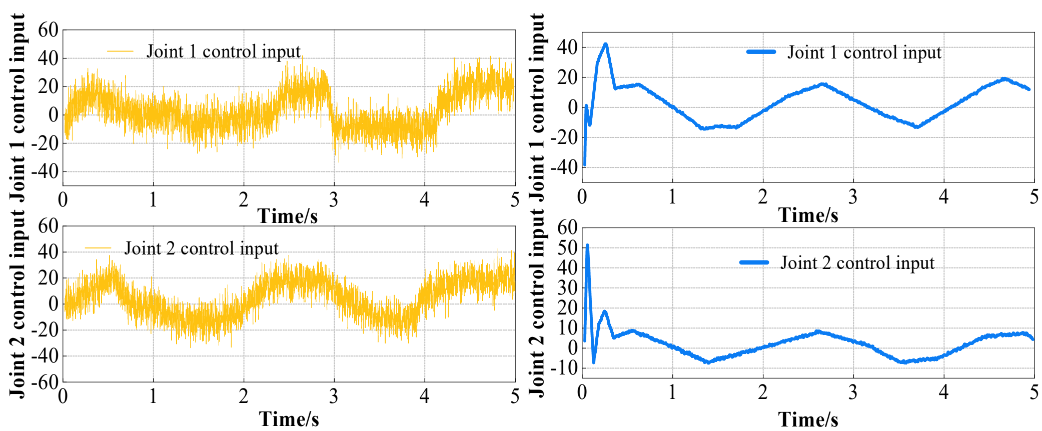

(a)Traditional method (b)Our method

Fig. 4. Joint control input

4. Robot vision-guided unloading experiment

This chapter builds a hand robot visual guidance unloading experimental platform, according to the designed fuzzy mathematics-based robot grasping control strategy, the particle swarm fuzzy PID controller is applied to the real item grasping process, and the robot visual guidance unloading experiments are carried out.

4.1. Experimental platforms

For the grasping task in unstructured scenes, this paper builds a robot grasping platform, which uses UR5 robotic arm and Robotiq2F parallel two-finger gripper as actuators, Intel RealSense D435 depth camera as the robot's "eyes", XELA The XR2144 3D haptic array sensor is used as the robot's "finger skin" to visually guide the perception of the grasping state.

4.2. Experimental design

The grasping objects come from the YCB dataset, which contains 15 different daily life objects with different shapes, sizes, and weights, and are denoted as G1~G15. In the single-target grasping experiments, one type of object from the set of grasping objects is selected in turn to form a scene, and the program is set to create 50 grasping scenes. The objects were randomly placed on the table, and their positional and orientation parameters were generated by random numbers, the placement position was within ±50 cm of the projected position of the camera, and the placement direction was rotated by rotating around the Z-axis. In the multi-target grasping experiment, five objects were randomly selected from the set of grasping objects to form a scene, and the program was set to create 50 grasping scenes.

After creating the scene, the visual perception system reasoned a set of grasping parameters, and the robot performed grasping the grasping point with the highest quality score, and only when the object was placed into the target tray, the robot would perform the next grasping, and the grasped objects would no longer appear on the desktop. In order to prevent the unsuccessful grasping in a certain scene leads to fall into a cycle of executing the grasping task, it is stipulated that when 3 consecutive unsuccessful grasps are made in the scene, the unloading task in this scene is terminated early.

4.3. Experimental results

Figure 5 shows the single target grab success rate and placement success rate. The overall grasping success rate is 92.51% and the placement success rate is 91.40%. The grasping success rate and placement success rate are shown in Table 1. The success rate of multi-target grasping is 87.54%, the placement success rate is 85.46%, and 288 out of 337 attempts of grasping objects are successfully placed in the target tray. The experimental results show that the robot is able to achieve a good average grasping success rate by performing the grasping task according to the particle swarm fuzzy PID control model.

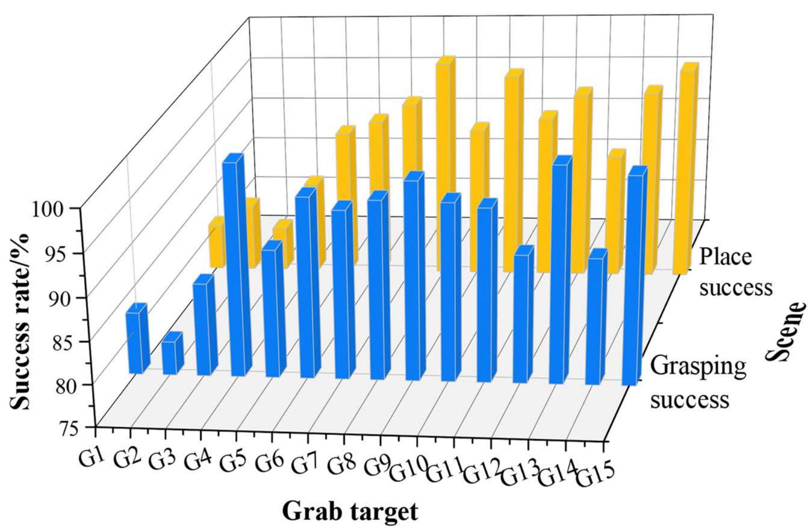

Fig. 5. Single goal capture success rate and placement success rate

Table 1. Grasping success rate and placement success rate

Grab scene	Robot grab	Result	Robot place	Result

Single target	Grasping number	814	Place number	814
	Grasping success	753	Place success	744
	Success rate/%	92.51%	Success rate/%	91.40%
Multi target	Grasping number	337	Place number	337
	Grasping success	295	Place success	288
	Success rate/%	87.54%	Success rate/%	85.46%

5. Conclusion

With the continuous development of robotics technology, relevant research is of great significance for the intelligent grasping and operating ability of robots in complex environments. In this paper, for the robot vision-guided unloading system, a robot unloading control model based on the fuzzy mathematical method is proposed, and the particle swarm algorithm is used to optimize the decision-making of the fuzzy PID control. The operational effect of the designed method is examined through simulation analysis of the model and robot unloading experiments. Compared with the traditional fuzzy PID control method, the method in this paper achieves better trajectory tracking effect, which can keep up with the desired trajectory within 0.5s, and the joint position error is almost 0, with faster convergence time, and at the same time, the system vibration phenomenon is greatly reduced. Using the method of this paper for robot unloading experiments, the success rate of single-target grasping and placing is 92.51% and 91.40%, respectively, and the success rate of multi-target grasping and placing is 87.54% and 85.46%, respectively. It shows that the particle swarm fuzzy PID control method has a good control effect on the robot unloading operation and can realize the accurate grasping and placing of items. In this paper, the stabilized grasping task of the robot is studied based on visual guidance, and although some research results have been achieved, the current strategy is relatively simple, and the grasping of complex stacked or highly intermixed objects has not yet been effectively solved. The future development of robot grasping technology requires interdisciplinary cooperation and innovation to better adapt to a variety of complex scenarios and to provide technical support for a wide range of robot applications in daily life, manufacturing and other fields.

Funding

1) This work was supported by Machine Vision Engineering Technology Center Project of Wuxi Vocational Institute of Commerce (KYPT21304).
2) Key Project of Wuxi Vocational Institute of Commerce in 2024: "Research on Teaching Methods of Electronic Technology Courses in Higher Vocational Education under Information Technology Conditions KJXJ24306".

References

[1] Lotti, N., Xiloyannis, M., Durandau, G., Galofaro, E., Sanguineti, V., Masia, L., & Sartori, M. (2020). Adaptive model-based myoelectric control for a soft wearable arm exosuit: A new generation of wearable robot control. IEEE Robotics & Automation Magazine, 27(1), 43-53.

[2] Wang, Z., Li, K., He, Q., & Cai, S. (2019). A light - powered ultralight tensegrity robot with high deformability and load capacity. Advanced Materials, 31(7), 1806849.

[3] Zhao, R., Bao, Z., Xiao, W., Zou, S., Zou, G., Xie, Y., & Leng, J. (2023). Fast Grasping Technique for Differentiated Mobile Phone Frame Based on Visual Guidance. Machines, 11(7), 689.

[4] Vicentini, F., Pedrocchi, N., Beschi, M., Giussani, M., Iannacci, N., Magnoni, P., ... & Fogliazza, G. (2020). Piros: Cooperative, safe and reconfigurable robotic companion for cnc pallets load/unload stations.

Bringing innovative robotic technologies from research labs to industrial end-users: the experience of the european robotics challenges, 57-96.

[5] Sun, Y., Wang, X., Lin, Q., Shan, J., Jia, S., & Ye, W. (2023). A high-accuracy positioning method for mobile robotic grasping with monocular vision and long-distance deviation. Measurement, 215, 112829.

[6] Leong, P. Y., & Ahmad, N. S. (2024). Exploring Autonomous Load-Carrying Mobile Robots in Indoor Settings: A Comprehensive Review. IEEE Access.

[7] Jung, E. J., Park, S., Kang, J. K., Son, S. E., Cho, G. R., & Lee, Y. (2022). Development of a Single-Arm Robotic System for Unloading Boxes in Cargo Truck. The Journal of Korea Robotics Society, 17(4), 417-424.

[8] Wenna, W., Weili, D., Changchun, H., Heng, Z., Haibing, F., & Yao, Y. (2022). A digital twin for 3D path planning of large-span curved-arm gantry robot. Robotics and Computer-Integrated Manufacturing, 76, 102330.

[9] Pieskä, S., Kaarela, J., & Mäkelä, J. (2018, April). Simulation and programming experiences of collaborative robots for small-scale manufacturing. In 2018 2nd international symposium on small-scale intelligent manufacturing systems (SIMS) (pp. 1-4). IEEE.

[10] Stilli, A., Wurdemann, H. A., & Althoefer, K. (2017). A novel concept for safe, stiffness-controllable robot links. Soft robotics, 4(1), 16-22.

[11] Zhou, G., Luo, J., Li, R., Xiang, K., Xu, S., Pang, M., ... & Zhang, S. (2021, September). A framework of industrial operations for hybrid robots. In 2021 26th International Conference on Automation and Computing (ICAC) (pp. 1-6). IEEE.

[12] Čech, M., Wicher, P., Lenort, R., Malčic, T., David, J., Holman, D., ... & Záruba, J. (2020). Autonomous mobile robot technology for supplying assembly lines in the automotive industry. Acta logistica, 7(2), 103-109.

[13] Farinelli, A., Zanotto, E., & Pagello, E. (2017). Advanced approaches for multi-robot coordination in logistic scenarios. Robotics and Autonomous Systems, 90, 34-44.

[14] Gao, R., Zhang, W., Wang, G., & Wang, X. (2023). Experimental research on motion analysis model and trajectory planning of GLT palletizing robot. Buildings, 13(4), 966.

[15] Merckaert, K., De Beir, A., Adriaens, N., El Makrini, I., Van Ham, R., & Vanderborght, B. (2018). Independent load carrying and measurement manipulator robot arm for improved payload to mass ratio. Robotics and Computer-Integrated Manufacturing, 53, 135-140.

[16] Tomo, T. P., Regoli, M., Schmitz, A., Natale, L., Kristanto, H., Somlor, S., ... & Sugano, S. (2018). A new silicone structure for uSkin—A soft, distributed, digital 3-axis skin sensor and its integration on the humanoid robot iCub. IEEE Robotics and Automation Letters, 3(3), 2584-2591.

[17] Gu, J., Wang, H., Pan, Y., & Wu, Q. (2015). Neural network based visual servo control for CNC load/unload manipulator. Optik, 126(23), 4489-4492.

[18] Stavrou, D., Timotheou, S., Panayiotou, C. G., & Polycarpou, M. M. (2017). Optimizing container loading with autonomous robots. IEEE Transactions on automation science and engineering, 15(2), 717-731.

[19] PANG, D. F., CUI, S. G., & LIU, X. (2021). Simulation design of robot loading and unloading workstation based on RobotStudio. Modular Machine Tool & Automatic Manufacturing Technique, 12, 129-131.

[20] Stoyanov, T., Vaskevicius, N., Mueller, C. A., Fromm, T., Krug, R., Tincani, V., ... & Echelmeyer, W. (2016). No more heavy lifting: Robotic solutions to the container unloading problem. IEEE robotics & automation magazine, 23(4), 94-106.

[21] Kadir, M. A., Chowdhury, M. B., Rashid, J. A., Shakil, S. R., & Rhaman, M. K. (2015, June). An autonomous industrial robot for loading and unloading goods. In 2015 International Conference on Informatics,

Electronics & Vision (ICIEV) (pp. 1-6). IEEE.

[22] Shen, D., Hu, J., Zhai, T., Wang, T., & Zhang, Z. (2019, October). Parallel loading and unloading: smart technology towards intelligent logistics. In 2019 IEEE International Conference on Systems, Man and Cybernetics (SMC) (pp. 847-851). IEEE.

[23] Hu, N. Z., Shi, Z. H., Hsu, K. H., Liu, S. W., Wu, R. W., Chuang, J. T., ... & Lee, J. D. (2021, October). Design a Fast Loading and Unloading Robot Controlling System by WebAPI Technique. In 2021 IEEE 3rd Eurasia Conference on IOT, Communication and Engineering (ECICE) (pp. 598-600). IEEE.

[24] Auh, E., Kim, J., Joo, Y., Park, J., Lee, G., Oh, I., ... & Moon, H. (2024). Unloading sequence planning for autonomous robotic container-unloading system using A-star search algorithm. Engineering Science and Technology, an International Journal, 50, 101610.

[25] Teng, Y., & Kang, X. (2023). The-Application-of-Servo-Control-Technology-in-Robot-Positioning-and-Tracking-System-via-Heuristic-Algorithm. Journal of Combinatorial Mathematics and Combinatorial Computing, 119, 277-289.